



## Effect of cerium ion (III) on corrosion resistance of organic–inorganic hybrid coating on surface of aluminum-tube used in refrigeration equipment

Wei XIAO<sup>1,2</sup>, Chang MIAO<sup>1,2</sup>, Xiong HUANG<sup>2</sup>, Rui-lin MAN<sup>2</sup>

1. College of Chemistry and Environmental Engineering, Yangtze University, Jingzhou 434023, China;
2. School of Chemistry and Chemical Engineering, Central South University, Changsha 410083, China

Received 4 November 2014; accepted 23 April 2015

**Abstract:** Organic–inorganic hybrid coating on the surface of aluminum-tube used in refrigeration equipment using cerium ion (III) as the additive was fabricated by sol–gel method, and the structure of the coating was confirmed by FT-IR. The results of the characterization show that the corrosion resistance of the coating with 1.5 mmol/L cerium ion (III) gains significant improvement, in which the colour retention time of CuSO<sub>4</sub> extends to 500 s, the anti-acid and alkali corrosion rates reduce by 67% and 70% compared with the blank one, respectively, and the salt spray tests also show good corrosion resistance. The electrochemical tests demonstrate that the self-corrosion current density and potential of the sample with hybrid coating are about  $2.877 \times 10^{-7}$  A/cm<sup>2</sup> and –0.550 V, respectively. The metallographic and SEM images show that the hybrid coating is uniform and dense, and the EDS analysis confirms that the coating is mainly composed of Al, Si and Ce elements.

**Key words:** aluminum-tube; organic–inorganic hybrid coating; corrosion resistance; cerium ion (III); refrigeration equipment

### 1 Introduction

Aluminum-tube is gradually used to replace copper-tube in the field of the refrigeration equipment because of its lighter mass and lower expense [1,2]. However, it is difficult for the aluminum-tube to sustain the long-term workload due to its inferior corrosion resistance. Although the surface of aluminum-tube has a thin layer oxide generated from its passivation, it can easily lose the function of protecting the stored food from the decomposition in the presence of corrosive medium in the refrigerator [3]. Therefore, it is very necessary to pretreat the aluminum-tube before being used to enhance the safety performance and extend the service life of the refrigeration equipment. It is well known that the chromating and anodizing processes have been widely and successfully employed to pretreat the surface of the matrix metal. However, the former is strictly prohibited due to the toxicity of the working solution containing hexavalent chromium to the human and environment, and the coating prepared by the latter is thick and brittle, which can be easily fractured and shed from the matrix material [1,4,5]. Therefore, it is

urgent to research and develop a practical and feasible process to enhance the corrosion resistance and protect the matrix metal.

In 1980s, HINTON and his co-workers [6,7] found that the novel coating with excellent corrosion resistance can be obtained on the surface of the aluminum alloy when the chloride containing rare earth element was deposited on the alloy matrix. The same results can be obtained for the magnesium alloy in Refs. [5,8,9]. However, the corrosion resistance decreased after long-time operation because the deposited rare earth coating was not uniform and dense, which cannot meet the practical requirements [10,11]. Silane as crosslinking agent is widely employed at present to improve the corrosion resistance of the surface of metal matrix because of its unique chemical structure, in which the silane can joint the metal matrix by forming the new Si—O—M (metal matrix) chemical bond and it can further develop into the three-dimensional network structure on the surface of the matrix by hydrolytic condensation and curing processes [12–15]. Hence, the prepared coating can improve the corrosion resistance by preventing the corrosive medium into the matrix. Considering the advantage and disadvantage of the single

silane coating and rare earth conversion coating, the novel organic–inorganic hybrid coating involving both silane and rare earth was proposed to improve the corrosion resistance of the metal matrix [16–18]. In the present work, the uniform and dense organic–inorganic hybrid coating with silane and rare earth element cerium on the surface of the aluminum-tube was prepared by sol–gel method and characterized by the physico-chemical methods, and the corrosion mechanism of the as-prepared hybrid coating was also investigated.

## 2 Experimental

### 2.1 Sample pretreatment and coating preparation

Aluminum-tube ( $d7.8 \text{ mm} \times 1 \text{ mm}$ ) used in the refrigeration equipments was provided by Changsha Hengjia Alcoa. Co., Ltd., and the chemical composition contains trace amounts of Fe, Cu, Si, Mn and Ti [15]. The aluminum-tube was pretreated prior to use according to the process described in the previous work [15].

Firstly, the working sol was prepared from a mixture of tetraethoxysilane and vinyltriethoxysilane (TEOS and VTES, provided by Sinopharm Chemical Reagent Co., Ltd.) in the presence of ammonia and appropriate concentration cerous nitrate according to hydrolysis processes [15,19]. Then, the desirable organic–inorganic hybrid coating on the surface of the aluminum-tube can be obtained by curing at  $120 \text{ }^\circ\text{C}$  for 1.5 h after the aluminum-tube being immersed into the working sol at  $40 \text{ }^\circ\text{C}$  for 1 min.

The chromate conversion coating on the surface of the aluminum-tube can be prepared by curing at  $100 \text{ }^\circ\text{C}$  for 1.5 h after the pretreated sample being soaked into a mixture of 5 g/L  $\text{CrO}_3$  and 3.5 g/L  $\text{Na}_2\text{Cr}_2\text{O}_7$  in the presence of the dilute nitric acid, which is denoted as chromate coating. For comparing, the aluminum-tube with only pretreatment was also studied and named as blank sample.

### 2.2 Properties characterization

Copper sulfate dropping test was considered as a practical method to evaluate the corrosion resistance of the coating because it can quickly reflect the grade of coatings by investigating the colour change of the drop, so it was utilized to optimize the added amount of cerous nitrate. The copper sulfate solution is a mixture of 50 g/L  $\text{CuSO}_4 \cdot 5\text{H}_2\text{O}$  and 50 g/L NaCl in the presence of diluted hydrochloric acid.

Alkali immersing mass loss and hydrogen evolution experiments were used to evaluate the anti-corrosion ability of surface coating in the alkaline and acid environment, respectively. In the alkaline solution, the corrosion rate of the sample can be calculated according to Eq. (1) after the sample being immersed

into 0.2 mol/L NaOH solution for 5 h, where  $v$  is the corrosion rate of the sample,  $m_0$  and  $m_1$  are the mass of the sample before and after immersion, respectively,  $S$  and  $t$  are the superficial area of the sample and the time of the anti-corrosion during the experiment, respectively. The volume of hydrogen gas was employed to characterize the corrosion rate in the acid solution. Hydrogen can be collected when the samples react with 3.0 mol/L HCl solution according to Eq. (2).

$$v = \frac{m_0 - m_1}{St} \quad (1)$$



Salt spray test can be accepted to determine the corrosion resistance of the metal material. Neutral salt spray (NSS) and copper-accelerated acetic acid-salt spray (CASS) tests were utilized to monitor the corrosion distribution of the samples with different coatings using YW–10 salt fog-box (ShangHai, China). According to the specification, 5% NaCl solution was atomized in a salt spray chamber at  $35 \text{ }^\circ\text{C}$  with the pH value of around 7 in the former, and the mixture of 5% NaCl and 0.02%  $\text{CuCl}_2$  solution in the presence of glacial acetic acid were atomized in a salt spray chamber at  $50 \text{ }^\circ\text{C}$  with the pH value of around 3 in the latter. The whole tested samples were placed at an angle of  $45^\circ$  in the chamber, exposed to the salt fog for a certain period. The formation of corrosion products was monitored by digital camera at different time.

Polarization and electrochemical impedance spectroscopy (EIS) measurements were used to investigate the corrosion mechanism of samples with different coatings [20,21]. Prior to test, the sample must be treated in the following steps. At first, the unexposed faces and edges of aluminum-tube were sealed with epoxy, leaving a working area of  $1.00 \text{ cm}^2$ . The specimens were pre-immersed in the 0.6 mol/L NaCl solution at pH value of 7 for 15 min before the data acquisition to achieve a steady state. In the three-electrode cell, a commercial saturated calomel electrode (SCE) and a platinum mesh were used as the reference and counter electrodes, respectively. On the average, three replicate samples were tested for each condition in every electrochemical test on a CHI660B electrochemical workstation purchasing from Chenhua Shanghai, China. Polarization test was used to measure the corrosion rate by evaluating polarization resistance from polarization curves, and the potential range was from the open circuit potential (OCP)–0.5 to OCP+0.5 V (vs SCE) with the scan rate of about 1 mV/s. EIS measurement was employed to monitor the corrosion performance of the sample in a naturally aerated 0.6 mol/L NaCl solution with pH value of 7, in which the

measured frequency ranged from  $10^{-2}$  to  $10^5$  Hz with an AC excitation amplitude of 10 mV.

The surface morphology of samples was observed using a 3DM metallographic microscope and an FEI Quanta 200 scanning electron microscope (SEM) equipped with an energy dispersive X-ray spectrometer (EDS) [22]. The accelerating voltage was 20 kV. To further investigate the mechanism, Fourier transform infrared (FT-IR) spectra were used to confirm the structure of the as-prepared sample with different coatings with a wavenumber resolution of  $2\text{ cm}^{-1}$  in the frequency range of  $4000\text{--}500\text{ cm}^{-1}$ .

### 3 Results and discussion

#### 3.1 Effect of cerium ion (III) concentration on corrosion resistance

The curve of different colour retention time of copper sulfate with different adding amounts of  $\text{Ce}(\text{NO}_3)_3$  is demonstrated in Fig. 1. It is observed that the colour retention time of  $\text{CuSO}_4$  solution extends with increasing the amount of  $\text{Ce}(\text{NO}_3)_3$  and can reach the maximum about 500 s when the doped concentration of cerium ion (III) is about 1.5 mmol/L. However, it is interesting to note that the colour retention time distinctly decreases with further increasing the concentration, which indicates that only appropriate amount cerium ion (III) is helpful to form the excellent anti-corrosion hybrid coating. Thus, the following elaborated study will be focused on the organic–inorganic hybrid coating with 1.5 mmol/L cerium ion (III).

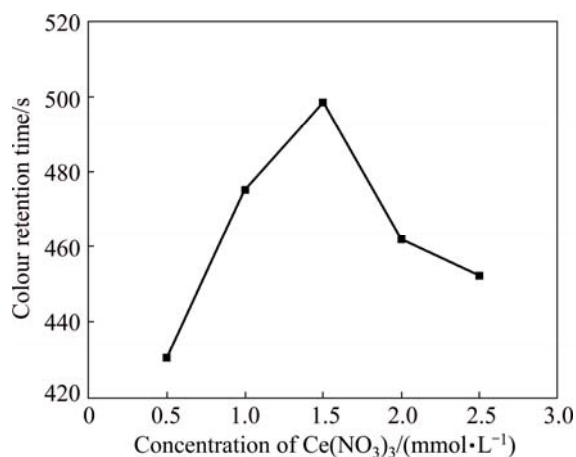


Fig. 1 Various colour retention time of  $\text{CuSO}_4$  with different adding amounts of  $\text{Ce}(\text{NO}_3)_3$

#### 3.2 Copper sulfate dropping

To compare with corrosion resistance of the as-prepared samples with different coatings on the surface of aluminum-tube, copper sulfate dropping experiments were also performed on them and the

corresponding results are listed in Table 1. It can be observed that the  $\text{CuSO}_4$  solution colour retention time shows much difference and the hybrid coating with cerium ion (III) can preserve the longest time about 500 s, which indicates that the hybrid coating may possess the best anti-corrosion performance.

Table 1 Results of copper sulfate dropping test of samples

Sample	Colour retention time of $\text{CuSO}_4$ solution/s			
	1st	2nd	3rd	Average time
Blank	13.0	11.0	12.0	12.0
Chromate coating	425.0	419.0	421.0	421.7
Hybrid coating with cerium ion (III)	500.0	503.0	499.0	500.7

#### 3.3 Alkali immersing mass loss

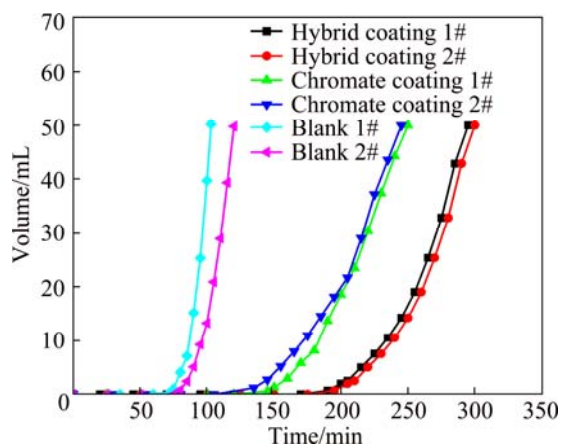
It is well known that the slower the corrosion rate is, the lower the corrosion degree of the matrix is. In other words, the excellent coating may show low corrosion rate under the same condition. Table 2 lists the results of alkali immersing mass loss of the samples with different coatings. Obviously, the samples with coating present much lower corrosion rate than the blank one. And the corrosion rate of the hybrid coating decreases to  $6.9327\text{ g}/(\text{m}^2\cdot\text{h})$ , about two-thirds of that of the blank one, which is in accordance with the results of the copper sulfate dropping experiments. The result may be attributed to the effective protection of the hybrid coating to the matrix by segregating the aluminum-tube matrix and NaOH corrosive medium.

Table 2 Results of alkali immersing mass loss of samples

Sample	$m_0/\text{g}$	$m_1/\text{g}$	$S/\text{m}^2$	$v/(\text{g}\cdot\text{m}^{-2}\cdot\text{h}^{-1})$
Blank	2.3548	2.1177	0.00230	20.6174
Chromate coating	2.3536	2.2177	0.00231	11.7769
Hybrid coating with cerium ion (III)	2.3340	2.2556	0.00226	6.9327

#### 3.4 Hydrogen evolution

Investigating the corrosion resistance of the as-prepared samples with different coatings in acid environment is also important for the aluminum-tube because it is often exposed to the acid medium resulting from the decomposition of stored food in the refrigerator. Hydrogen evolution is usually utilized to evaluate the anti-acid ability by comparing the rates of releasing hydrogen for the samples under the same condition. The hydrogen volume as a function of time for various samples is given in Fig. 2. It is observed from Fig. 2 that the plots present much difference during the whole process, in which the releasing hydrogen rates of the



**Fig. 2** Results of hydrogen evolution test of samples

samples with coatings are much slower than that of the blank one, and that of the sample with cerium ion (III) doped hybrid coating is the lowest. The results may be attributed to the coatings on the surface of the matrix,

which can slow down the reactions between the aluminum-tube matrix and HCl medium. It is worthy to note that the anti-acid performance of the hybrid coating is even superior to that of the chromate coating.

### 3.5 Salt spray test

Figures 3 and 4 present the digital images of the aluminum-tubes with different coatings, which are characterized by the NSS and CASS tests, respectively. When the samples are exposed to the salt spray tests, there are more and more pittings on the surface of the matrix and the metallic luster of the matrix becomes weaker as the time goes. It can be observed from the fact that the anti-corrosion time of the samples with chromate coating and hybrid coating are much longer than that of the blank one in both the NSS and CASS tests, which suggests that the samples with coatings can well endure corrosion when exposed to the aggressive medium. Furthermore, the samples in the CASS test present more serious corrosion than those in the NSS test at the

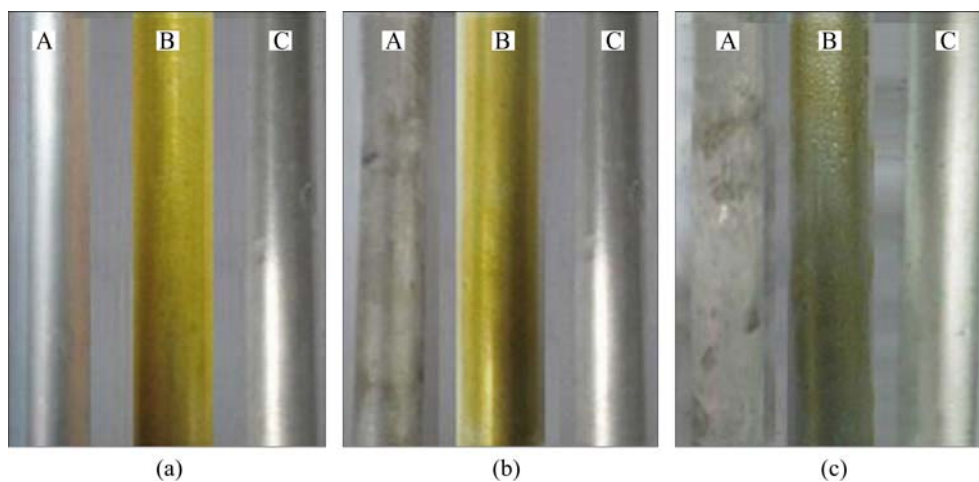


**Fig. 3** Digital images of samples with different coatings after NSS test for 0 (a), 30 h (b) and 240 h (c) (A: Blank; B: Chromate coating; C: Hybrid coating with cerium ion (III))

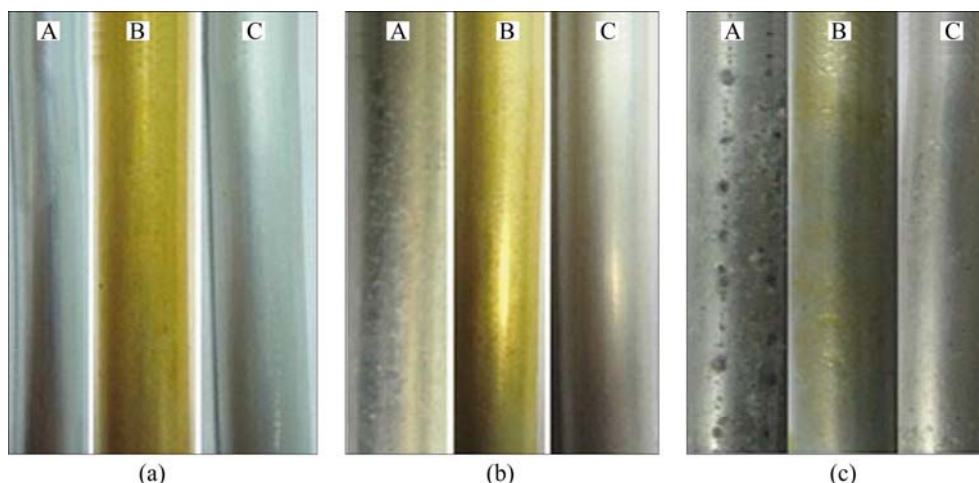


**Fig. 4** Digital images of samples with different coatings after CASS test for 0 (a), 4 h (b) and 24 h (c) (A: Blank; B: Chromate coating; C: Hybrid coating with cerium ion (III))

beginning tested time, which can be attributed to others corrosion reactions for the aluminum matrix in the latter and accelerate the corrosion of the matrix.

### 3.6 Electrochemical tests

The polarization curves of the samples with different coatings are displayed in Fig. 5. It can be seen that the curves of the samples with and without coating have the same trend, which agrees with Ref. [23]. The same shape of the curves may suggest that the samples with different coatings have similar corrosion mechanism. However, the slopes of curves present differences, which indicates that the corrosion degree of the matrix is different. To well investigate the corrosion mechanism of the coatings, the polarization curves are fitted by the C-view software and the corresponding results are listed in Table 3. Obviously, the sample with hybrid coating possesses the lowest self-corrosion current density of  $2.877 \times 10^{-7} \text{ A/cm}^2$ , which decreases by one and two orders of magnitude compared with that of the chromate coating and blank sample, respectively. The results indicate that the corrosion of the matrix is effectively inhibited by decreasing the self-corrosion current density. The self-corrosion potential is another parameter to determine the corrosion degree of the samples, in which the higher the potential is, the better the anti-corrosion of coating is. It can be obtained from Table 3 that the self-corrosion potential increases when the coating is deposited on the matrix, in which the value increases from  $-0.728 \text{ V}$  for the blank sample to  $-0.666 \text{ V}$  for the chromate coating sample, and up to  $-0.550 \text{ V}$  for the hybrid coating sample with cerium ion (III). The results suggest that the corrosion resistance gains much improvement from another perspective, which can be explained that the hybrid coating on the surface of aluminum-tube can effectively restrain the electrochemical reactions on the interface by preventing the extrinsic medium into the matrix to slow down the electrochemical corrosion rate.

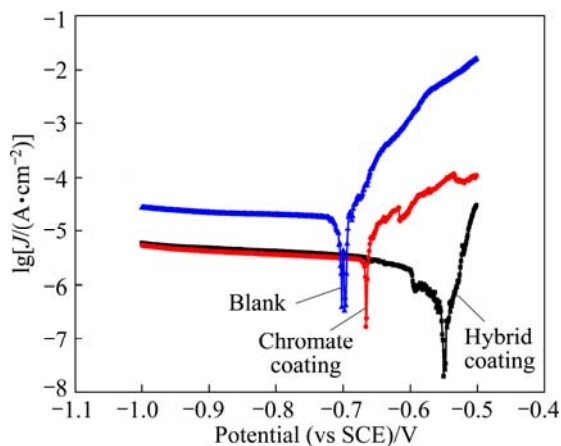


Fig. 5 Polarization curves of samples with different coatings

Table 3 Fitting results of polarization curves

Sample	Self-corrosion current density/ $(10^{-7} \text{ A} \cdot \text{cm}^{-2})$	Self-corrosion potential/V
Blank	155.6	-0.728
Chromate coating	29.04	-0.666
Hybrid coating with cerium ion (III)	2.877	-0.550

The EIS spectra of different samples soaked into  $0.6 \text{ mol/L NaCl}$  solution with pH value of 7 for 15 min are displayed in Fig. 6. According to Refs. [15,16,20], the resistance value at low frequency is the simple parameter to evaluate the anti-corrosion performance of the electrode. It can be observed from Fig. 6(a) that the resistance value at low frequency about  $10^{-2} \text{ Hz}$  presents differences, in which the value increases from  $5.5 \text{ k}\Omega \cdot \text{cm}^2$  for the blank sample to  $31.6 \text{ k}\Omega \cdot \text{cm}^2$  for the chromate coating sample, and to the maximum about  $40.0 \text{ k}\Omega \cdot \text{cm}^2$  for the organic-inorganic hybrid coating sample. The results indicate that the corrosion resistance of the sample with coating gains much improvement, especially with the hybrid coating. To further investigate the corrosion mechanism of the coating, Fig. 6(b) demonstrates the phase angle diagrams of different samples under the same condition. Obviously, there are

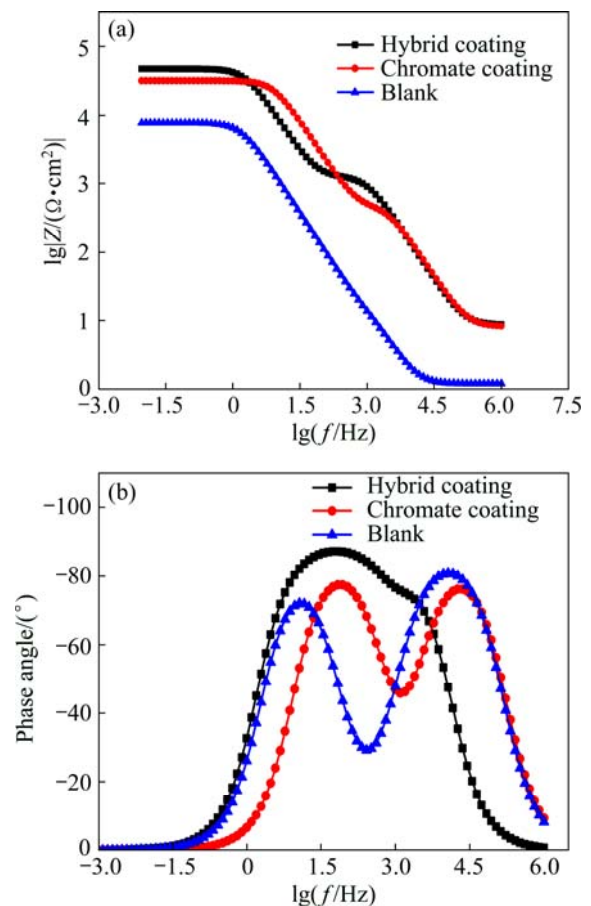
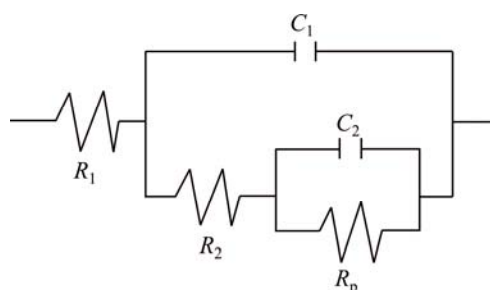


Fig. 6 EIS Bode plots of samples with different coatings: (a) Frequency impedance; (b) Phase angle

still two peaks for each plot, which can be depicted as time constant. One appearing at higher frequency about  $10^3$  Hz with a maximum phase angle around  $-80^\circ$  can be assigned to the formation of a passivation coating on the surface of the aluminum-tube, and the other at lower frequency about 10 Hz with a phase angle around  $-70^\circ$  corresponds to the corrosion onset, as reported in Refs. [8,11,15,20]. It is worthy to note that the phase angle of the hybrid coating is around  $-90^\circ$  in higher frequency and the two peaks gradually evolve into the whole one, which suggests that the behavior of the hybrid coating is close to the capacitor. Furthermore, the corresponding equivalent circuit of the hybrid coating is presented in Fig. 7, which can be described as  $R_1$  in series with parallel  $\{C_1(R_2(C_2R_p))\}$  element  $\{R_1(C_1(R_2(C_2R_p)))\}$ , wherein,  $R_p$  is the resistance value of



**Fig. 7** Equivalent circuit diagram of EIS plots of sample with hybrid coating

the solution,  $R_1$  and  $R_2$  are the resistance values of the outer and the inner of the sample with hybrid coating, respectively,  $C_1$  and  $C_2$  are the capacitors of the solution and the coating, respectively. The fitting value of  $R_p$  of the hybrid coating is about  $39.8 \text{ k}\Omega\cdot\text{cm}^2$ , which is close to the tested value. The results also prove that the hybrid coating with cerium ion (III) can provide excellent protection for the aluminum matrix.

### 3.7 Surface morphology

The metallographic and SEM images of the samples with different coatings are demonstrated in Fig. 8. It can be observed that the surface of the samples presents much difference and there is a layer of thin coating on the surface of the aluminum-tube matrix, which can prevent the matrix from corrosion. It is worthy to note that the thickness of coating in Fig. 8(c) is thinner than that in Fig. 8(b), which suggests that the coating in Fig. 8(c) may provide better adhesion to the aluminum-tube matrix. In order to further investigate the composition of the hybrid coating, the SEM image and EDS pattern of selected area are shown in Fig. 8(d). It can be seen from Fig. 8(d) that the surface is uniform and dense, which may be attributed to the coating deposited by the cerium ion (III). The results can be confirmed by the EDS results of the selected area 1 in the hybrid coating, which shows that the coating is mainly composed of Al, Si and Ce elements.

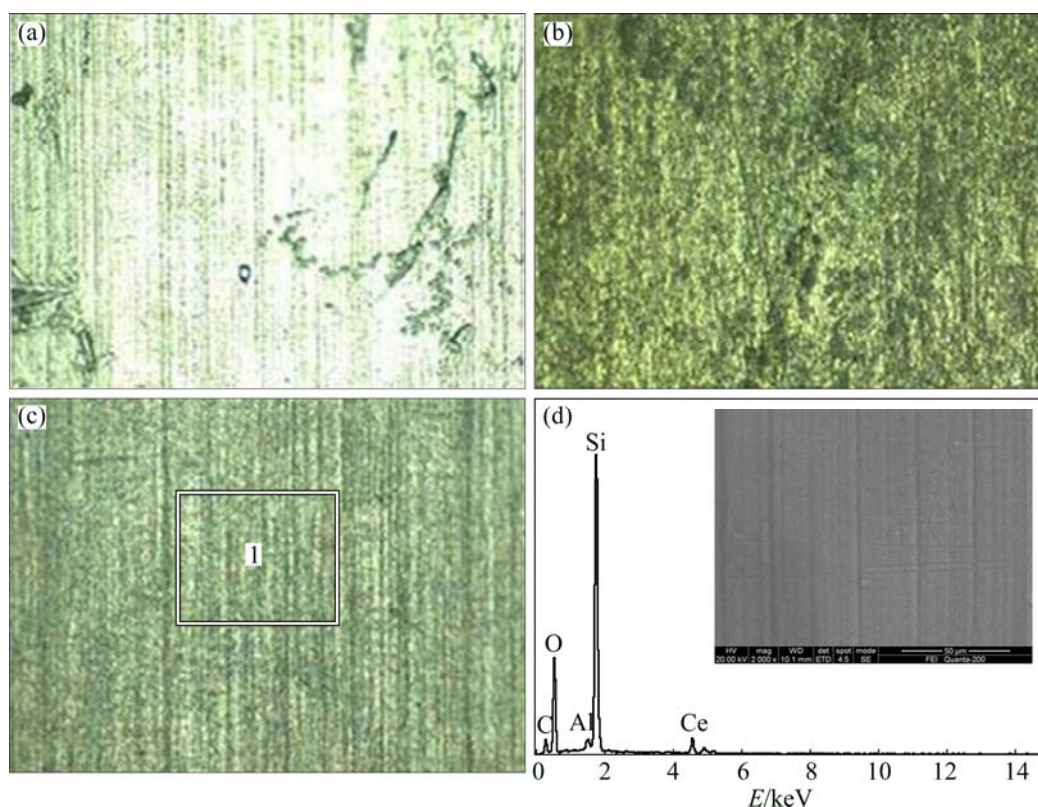
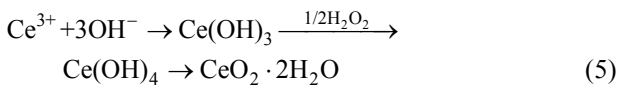
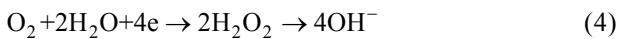


**Fig. 8** Metallographic images of surface of samples with only pretreatment (a), chromate coating (b), hybrid coating with cerium ion (III) (c), and SEM image and EDS pattern of selected area 1 of hybrid coating (d)

### 3.8 Mechanism analysis

The hybrid coating on the surface of the matrix was prepared when the pretreated aluminum-tube was placed into the silane working sol with cerium ion (III) for some time. From the above analysis, the hybrid coating can provide protection for the aluminum-tube matrix and possesses excellent corrosion resistance, which can be partly attributed to the deposition of cerium ion (III) on the matrix, and partly to the formation of new three-dimensional network on the surface of the matrix.



When the sample with hybrid coating is confronted with the corrosive medium, there are many electrochemical reactions on the surface of the matrix due to the formation of micro-corrosion batteries. On one hand, the anode dissolution and cathode reduction reactions listed in Eqs. (3) and (4) can readily happen [15,20]. The deposition reactions on the surface of the matrix proceed when the pH value of the solution increases to 8, which results from the reduction reactions on the cathode. The increased pH value of the solution is helpful to form the ceric oxide on the surface of the aluminum-tube in the presence of oxygen according to Eq. (5), which was demonstrated by the schematic diagram in the previous work [15]. On the other hand, a new three-dimensional network on the surface of the matrix may form by depositing cerium ion (III) into the silane network and the desired dense and uniform hybrid coating can be obtained after curing, which are demonstrated in Fig. 9. The results are confirmed by FT-IR spectrum shown in Fig. 10. It can be seen from Fig. 10 that the sharp peaks appearing at 1057 and 1415.21  $\text{cm}^{-1}$  are assigned to the characteristic peaks of Si—O—Si for the hydrolysis and C=C double bond for the VTES, respectively. It is worthy to note that the peaks at around 860 and 446  $\text{cm}^{-1}$  can be attributed to the stretching vibration peaks of Ce—O and Si—O bond, respectively. These results may provide reasonable evidences that the cerium was successfully grafted on the network by the silane. The absorption peak at around 3429  $\text{cm}^{-1}$  may be assigned to the O—H bond for the absorbed water.

### 4 Conclusions

1) Organic–inorganic hybrid anti-corrosion coating with cerium ion (III) on the surface of aluminum-tube was prepared via sol–gel method.

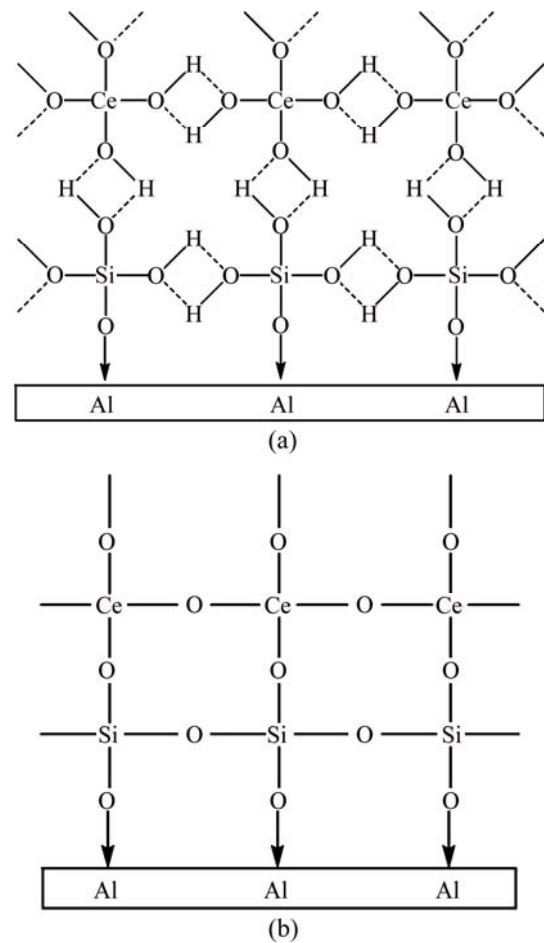


Fig. 9 Structural diagrams of hybrid coating before (a) and after (b) curing

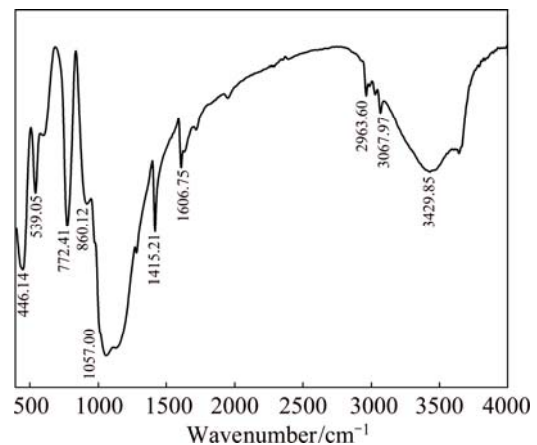


Fig. 10 FT-IR spectrum of hybrid coating with cerium ion (III)

2) The results of the characterization suggest that the as-prepared hybrid coating possesses excellent anti-corrosion performance, such as excellent acid and alkali resistance, and prolonged anti-salt spray ability.

3) The results of the mechanism analysis show that the new three-dimensional network forms on the surface of the matrix and can improve the corrosion resistance of the aluminum-tube.

## References

- [1] CARNEIRO J, TEDIM J, FERNANDES S C M, FREIRE C S R, SILVESTRE A J D, GANDINI A, FERREIRA M G S, ZHELUDKEVICH M L. Chitosan-based self-healing protective coatings doped with cerium nitrate for corrosion protection of aluminum alloy 2024 [J]. Progress in Organic Coatings, 2012, 75(1): 8–13.
- [2] ATRENS A, SONG G L, LIU M, SHI Z, CAO F, DARGUSCH M S. Review of recent developments in the field of magnesium corrosion [J]. Advanced Engineering Materials, 2015, 17(4): 400–453.
- [3] DECK P D, MOON M, SUJDAK R J. Investigation of fluoacid based conversion coatings on aluminum [J]. Progress in Organic Coatings, 1997, 34(1): 39–48.
- [4] FENG L, ZHANG H, WANG Z, LIU Y. Superhydrophobic aluminum alloy surface: Fabrication, structure, and corrosion resistance [J]. Colloids and Surfaces A: Physicochemical and Engineering Aspects, 2014, 441: 319–325.
- [5] LI X D, WANG X S, REN H H, CHEN Y L, MU Z T. Effect of prior corrosion state on the fatigue small cracking behaviour of 6151-T6 aluminum alloy [J]. Corrosion Science, 2012, 55: 26–33.
- [6] HINTON B R W, WILSON L. The corrosion inhibition of zinc with cerous chloride [J]. Corrosion Science, 1989, 29(8): 967–985.
- [7] HINTON B R W. Corrosion inhibition with rare earth metal salts [J]. Journal of Alloys and Compounds, 1992, 180(1): 15–25.
- [8] LAMAKA S V, XUE H B, MEIS N N A H, ESTEVES A C C, FERREIRA M G S. Fault-tolerant hybrid epoxy–silane coating for corrosion protection of magnesium alloy AZ31 [J]. Progress in Organic Coatings, 2015, 80: 98–105.
- [9] CHEN J Y, CHEN X B, LI J L, TANG B, BIRBILIS N, WANG X. Electro sprayed PLGA smart containers for active anti-corrosion coating on magnesium alloy Amlite [J]. Journal of Materials Chemistry A, 2014, 2(16): 5738–5743.
- [10] FAHIMPOUR V, SADRNEZHAAD S K, KARIMZADEH F. Corrosion behavior of aluminum 6061 alloy joined by friction stir welding and gas tungsten arc welding methods [J]. Materials & Design, 2012, 39: 329–333.
- [11] SEIFZADEH D, BEZAATPOUR A, JOGHANI R A. Corrosion inhibition effect of N,N'-bis(2-pyridylmethylidene)-1,2-diiminoethane on AZ91D magnesium alloy in acidic media [J]. Transactions of Nonferrous Metals Society of China, 2014, 24(11): 3441–3451.
- [12] BETHENCOURT M, BOTANA F J, CANO M J, MARCOS M. High protective, environmental friendly and short-time developed conversion coatings for aluminium alloys [J]. Applied Surface Science, 2002, 189(1): 162–173.
- [13] ZUCCHI F, GRASSI V, FRIGNANI A, TRABANELLI G. Inhibition of copper corrosion by silane coatings [J]. Corrosion Science, 2004, 46(11): 2853–2865.
- [14] CABRAL A M, DUARTE R G, MONTEMOR M F, FERREIRA M G S. A comparative study on the corrosion resistance of AA2024-T3 substrates pre-treated with different silane solutions: Composition of the films formed [J]. Progress in Organic Coatings, 2005, 54(4): 322–331.
- [15] XIAO Wei, MAN Rui-lin, MIAO Chang, PENG Tian-lan. Study on corrosion resistance of the BTESPT silane cooperating with rare earth cerium on the surface of aluminum-tube [J]. Journal of Rare Earths, 2010, 28(1): 117–122.
- [16] PALANIVEL V, HUANG Y, van OOIJ W J. Effects of addition of corrosion inhibitors to silane films on the performance of AA2024-T3 in a 0.5 M NaCl solution [J]. Progress in Organic Coatings, 2005, 53(2): 153–168.
- [17] PALOMINO L M, SUEGAMA P H, AOKI I V, MONTEMOR M F, de MELO H G. Electrochemical study of modified cerium–silane bi-layer on Al alloy 2024-T3 [J]. Corrosion Science, 2009, 51(6): 1238–1250.
- [18] FAYOMI O S I, POPOOLA A P I. In-situ formation characteristic, tribological characterization and anti-corrosion properties of quaternary composites films [J]. Transactions of Nonferrous Metals Society of China, 2014, 24(10): 3170–3180.
- [19] XIAO W, LI X H, GUO H J, WANG Z X, ZHANG Y H, ZHANG X P. Preparation of core-shell structural single ionic conductor  $\text{SiO}_2@Li^+$  and its application in PVDF–HFP-based composite polymer electrolyte [J]. Electrochimica Acta, 2012, 85: 612–621.
- [20] CAMPETRINI P, van WESTING E P M, DEWIT J H W. Influence of surface preparation on performance of chromate conversion coatings on Alclad 2024 aluminium alloy. Part II: EIS investigation [J]. Electrochimica Acta 2001, 46(17): 2631–2647.
- [21] ZHANG Xin, LI Yong-jun, ZHANG Kui, WANG Chang-sun, LI Hong-wei, MA Ming-long, ZHANG Bao-dong. Corrosion and electrochemical behavior of Mg–Y alloys in 3.5% NaCl solution [J]. Transactions of Nonferrous Metals Society of China, 2013, 23(5): 1226–1236.
- [22] WU Hong-yan, LIU Jian, ZHAO Hao-feng, JIANG Qiang, XU Yi, XU Jia. Effect of surface microstructure of aluminum coating on corrosion properties of magnetic refrigerant gadolinium [J]. Transactions of Nonferrous Metals Society of China, 2013, 23(11): 3280–3285.
- [23] IMAZ N, OSTRAL M, VIDAL M, DIEZ J A, SARRET M, GARCIA-LECINA E. Corrosion behaviour of chromium coatings obtained by direct and reverse pulse plating electrodeposition in NaCl aqueous solution [J]. Corrosion Science, 2014, 78: 251–259.

## 三价铈离子对制冷设备用铝管表面有机–无机杂化膜耐蚀性能的影响

肖 围<sup>1,2</sup>, 缪 畅<sup>1,2</sup>, 黄 雄<sup>2</sup>, 满瑞林<sup>2</sup>

1. 长江大学 化学与环境工程学院, 荆州 434023; 2. 中南大学 化学化工学院, 长沙 410083

**摘 要:** 采用溶胶–凝胶法在制冷设备用铝管表面制备三价铈离子作为添加剂的有机–无机杂化膜, 通过傅里叶变换红外光谱确认其结构。性能测试结果表明: 当三价铈离子浓度达到 1.5 mmol/L 时, 所得到的杂化膜的耐蚀性能有明显的改善; 与空白试样相比, 其中  $\text{CuSO}_4$  的变色时间延长到 500 s, 耐酸和耐碱腐蚀速率分别降低了 67% 和 70%, 盐雾试验结果也表现出很好的耐蚀性。电化学测试表明, 杂化膜试样的自腐蚀电流密度和自腐蚀电压分别为  $2.877 \times 10^{-7} \text{ A/cm}^2$  和  $-0.550 \text{ V}$ 。金相和扫描电镜图片显示杂化膜均匀致密。X 射线能谱分析表明该膜层主要由 Al、Si 和 Ce 等元素组成。

**关键词:** 铝管; 有机–无机杂化膜; 耐蚀性能; 三价铈离子; 制冷设备

(Edited by Mu-lan QIN)